https://doi.org/10.5194/egusphere-2025-6541
Preprint. Discussion started: 12 February 2026

Parameterization and Evaluation of Nonhydrostatic Effect in the Orographic Gravity Wave Drag in China Meteorological Administration Global Forecast System (CMA-GFS) v4.0 Model

Rongrong ZHANG[1,2,3], Zhenzhen AI[1], Xin XU[1], Haile XUE[4,5], Qiying CHEN[4,5]

[1]State Key Laboratory of Severe Weather Meteorological Science and Technology, Key laboratory of Mesoscale Severe Weather/Ministry of Education, School of Atmospheric Sciences, Nanjing University, Nanjing 210023, China
[2]Jiangsu Meteorological Observatory, Jiangsu Meteorological Bureau, Nanjing 210000, China
[3]Jiangsu Key Laboratory of Severe Storm Disaster Risk/Key Laboratory of Transportation Meteorology of CMA, Nanjing 210000, China
[4]State Key Laboratory of Severe Weather Meteorological Science and Technology, CMA Earth System Modeling and Prediction Centre, Beijing 100081, China
[5]Key Laboratory of Earth System Modeling and Prediction, China Meteorological Administration, Beijing 100081, China

Correspondence: Xin Xu (xinxu@nju.edu.cn) and Haile Xue (xuehl@cma.cn)

https://doi.org/10.5194/egusphere-2025-6541
Preprint. Discussion started: 12 February 2026

Abstract

The China Meteorological Administration Global Forecast System (CMA-GFS) v4.0 model was upgraded to a higher resolution of 0.125° in May 2023. To be compatible with its fine resolution, the parameterization scheme of orographic gravity wave drag (OGWD) in CAM-GFS is revised herein by accounting for the nonhydrostatic effect (NHE) on the wave momentum flux of subgrid-scale orographic gravity waves. The performance of the revised OGWD scheme is then evaluated for the 10-day medium-range forecast in December 2023. Results show that the revised OGWD scheme can better capture the large-scale circulation in the Northern Hemisphere (NH), particularly in the high latitudes. The easterly (westerly) wind biases in the NH polar stratosphere (troposphere) are decreased. The underestimation of East Asia subtropical jet is also alleviated. Quantitative evaluation shows that the revised OGWD scheme reduces both the mean bias and root mean square error of 500-hPa geopotential height in the NH after the 6th forecast day, reaching 11.59% and 5.06%, respectively, by day 10. The decrease of easterly biases in the polar stratosphere is owing to the weakening of stratospheric zonal OGWD by the NHE. It is also contributed by the secondary circulation induced by the weakened OGWD, which increases the thermal contrast between middle and high latitudes by adiabatic warming/cooling. For the decrease of westerly biases in the NH polar troposphere, it is due to the fact that the enhanced stratospheric winds suppress the upward propagation of Rossby waves into the stratosphere, resulting in greater convergence of Eliassen-Palm flux in the mid-upper troposphere.

Keywords: orographic gravity wave drag, parameterization, global NWP medium-range forecast

https://doi.org/10.5194/egusphere-2025-6541
Preprint. Discussion started: 12 February 2026

1. Introduction

Orographic gravity wave drag (OGWD) is an important process in atmospheric dynamics, arising from the interaction of airflow with complex terrain (Kim et al., 2003; Teixeira, 2014). When airstream flows over mountains, it generates orographic gravity waves (OGWs) which propagate vertically, when breaking transferring momentum from the surface to higher levels (Fritts and Alexander, 2003). This momentum transfer plays a crucial role in driving the atmospheric circulation, influencing both tropospheric and stratospheric dynamics (Alexander et al., 2010).

In numerical weather prediction (NWP) and climate models, the OGWD is typically a subgrid-scale process which needs to be parameterized. Various OGWD parameterization schemes have been developed over the past few decades (e.g., Palmer et al., 1986; McFarlane, 1987; Kim and Arakawa, 1995; Lott and Miller, 1997; Scinocca and McFarlane, 2000; Kim and Doyle, 2005) based on both linear and nonlinear OGW dynamics. Their implementation has been shown to help alleviate the systematic biases in both NWP and climate models, ranging from general circulation to regional climate and weather (e.g., Kim, 2007; McLandress et al., 2012; Choi and Hong, 2015; Zhong and Chen, 2015; Chen et al., 2016; Lu et al., 2020; Zhang et al., 2020; Li et al., 2023; Xu et al., 2023; Wei et al., 2025).

While accurate representation of OGWD is essential for weather forecast and climate simulation/projection, traditional OGWD parameterization schemes rely on the assumption of hydrostatic balance which can significantly simplify the formulae of OGW dynamics. This assumption is appropriate for coarse-resolution numerical models where subgrid-scale OGWs are dominated by hydrostatic GWs as the dominant subgrid

https://doi.org/10.5194/egusphere-2025-6541
Preprint. Discussion started: 12 February 2026

"mountains" are large. However, as the model resolution increases, the hydrostatic assumption becomes less valid because the subgrid-scale orography (SSO) becomes smaller, so that the unresolved GWs have shorter wavelengths. In this situation, the nonhydrostatic effects (NHEs) will exert remarkable influences on the subgrid-scale OGWs. [Note that NHE should also affect the OGWD in coarser-resolution models but only has a weaker impact. This is because subgrid OGWs are generally in hydrostatic balance in coarser-resolution models, with very few momentum fluxes being carried by nonhydrostatic OGWs.] For example, nonhydrostatic OGWs propagate more laterally than hydrostatic ones. The horizontal dispersion of wave energy can reduce the wave amplitude (Smith, 1979; Klemp and Durran, 1983; Zängl, 2003), which substantially suppresses gravity wave breaking and the deposition of wave momentum into the mean flow. These NHEs are thus critical for accurately representing the dynamical impacts of subgrid-scale OGWs in high-resolution models, e.g., the *state-of-the-art* global NWP models.

Recently, Xu et al. (2021) theoretically derived the analytical expressions for the surface wave momentum flux (WMF) of nonhydrostatic OGWs generated by idealized three-dimensional orography. They found that the degree of nonhydrostaticity can be measured by a nondimensional parameter of Froude number which is equal to the wind speed over the mountain half width and buoyancy frequency. Physically, this parameter represents the ratio between the period of buoyancy oscillation and the time for airflow travelling through the mountain. The larger the horizontal Froude number, the more important the NHE is. Based upon the theoretical study, Xu et al. (2023, 2024) revised the OGWD parameterization scheme developed by Kim and Doyle (2005,

https://doi.org/10.5194/egusphere-2025-6541
Preprint. Discussion started: 12 February 2026

hereafter KD05) by accounting for the NHE on the surface WMF of upward-propagating OGWs. Then the new OGWD scheme was implemented in the Model for Prediction Across Scales (MPAS), which was shown to improve the seasonal simulation of the stratospheric polar night jet and reduce the wet biases over the western Tibetan Plateau in winter. Li et al. (2024) further evaluated the revised OGWD scheme in the Weather Research and Forecasting (WRF) model for short-range forecast of Northeast China cold vortices (NECVs). The underestimation of the NECV intensity (in terms of minimum 500-hPa geopotential height) is alleviated as the NHE decreases the lower-tropospheric OGWD.

The China Meteorological Administration Global Forecast System (CMA-GFS) is a rename of the Global/Regional Assimilation and Prediction System (GRAPES) developed in early 2000s (Shen et al., 2017). Operationally running at the CMA Earth System Modeling and Prediction Center, the CMA-GFS was upgraded to a new version of v4.0 in May 2023, with its horizontal resolution increasing from about 0.25° to 0.125° (about 13 km), along with many other improvements in the model dynamics and physics. For instance, the convective triggering function and quasi-equilibrium closure conditions are improved to reduce biases in tropics and enhance forecast skill of precipitation in East Asia. In CMA-GFS, three components of subgrid orographic effects have been implemented, i.e., the blocking-flow drag (BFD), the OGWD and turbulent orographic form drag (TOFD). The TOFD scheme was implemented CMA-GFS based on Beljaars et al. (2004) and Xue et al. (2011) and will not be further discussed as it is not relevant to the NHE effect studied in this study. The BFD component based on Lott and Millor (1997, hereafter LM97) and OGWD component

https://doi.org/10.5194/egusphere-2025-6541
Preprint. Discussion started: 12 February 2026

112 from Kim and Arakawa (1995, hereafter KA95) were implemented in CMA-GFS
113 similar to that in Alpert (2004) and was descripted in Chen et al. (2016). It is noticed
114 that the NHE effects were partially considered in KA95 by partitioning the momentum
115 stress with the Scorer parameter when model grid mainly locates at the downstream of
116 the subgrid orography. However, the surface OGWD remains with the original KA95
117 scheme. In order to be compatible with its high resolution, this hydrostatic OGWD
118 parameterization scheme needs to be upgraded to account for the NHE.

119 Note that the present study extends the evaluation of the nonhydrostatic OGWD
120 scheme in the MPAS model presented in Xu et al. (2024) by transitioning it into a
121 practical, operational NWP. Although Xu et al. (2024) demonstrated the beneficial
122 impact of the revised OGWD scheme for long-term, large-scale circulation simulations,
123 its performance and value within a state-of-the-art, high-resolution global forecasting
124 system performing routine medium-range forecasts had not been tested. This work
125 provides this critical assessment using the CMA-GFS v4.0 model, with a specific focus
126 on forecast skill improvements for several quantitative metrics. The primary advance
127 lies in evaluating the revised OGWD scheme in reducing systematic forecast biases on
128 timescales directly relevant to weather prediction (1-10 days). Therefore, this research
129 bridges the gap between parameterization development and operational implementation,
130 demonstrating the tangible benefits of incorporating nonhydrostatic effects to improve
131 medium-range weather forecasting accuracy.

132 The remainder of the paper is organized as follows. Section 2 firstly introduces
133 the revision of the OGWD parameterization scheme and then describes the setup of the
134 numerical experiments. Section 3 gives an overall evaluation for the medium-range

https://doi.org/10.5194/egusphere-2025-6541
Preprint. Discussion started: 12 February 2026

forecast of large-scale atmospheric circulation by the CMA-GFS model. The NHE effects on parameterized OGWD and large-scale circulation are examined in section 4. Finally, the paper is summarized in section 5 along with discussions.

2. OGWD parameterization scheme and numerical experiments

a. Revision of the KA95 OGWD parameterization scheme

The KA95 OGWD considers various aspects of the SSO including its standard deviation (σ_h), orographic asymmetry (OA) and orographic convexity (OC). The surface WMF of OGWs is given by

$$\tau_0 = \rho_0 E \frac{m}{\lambda_{eff}} G \frac{|V_0|^3}{N_0}, \quad (1)$$

where

$$E = (OA + 2)^{C_E \frac{Fr_0}{Fr_c}}, m = (1 + L_x)^{OA+1}, G = \frac{Fr_0^2}{Fr_0^2 + C_G OC^{-1}}, Fr_0 = \frac{\sigma_h N_L}{|\mathbf{V}_L|}. \quad (2)$$

The variables ρ_0, $|\boldsymbol{V_0}|$ and N_0 are the low-level mean air density, horizontal wind speed and buoyancy frequency. The parameter m denotes the "number of mountains" within the grid cell, characterizing the total volume of SSO associated with the orography length (L_x). The coefficient λ_{eff} acts as a tunable parameter denoting the effective grid length. The transition function G is an enhancement factor for sharp mountains as OC is large. This scheme also considers the effects of low-level wave breaking and/or lee wave trapping through the factor E, which is a function of the shape and location of the SSO within the model grid cell (i.e., OA), and the flow nonlinearity (i.e., Fr_0). The two constants are set to C_E = 0.8 and C_G = 0.5, which are obtained empirically through a series of numerical simulations conducted in Kim and Arakawa (1995).

https://doi.org/10.5194/egusphere-2025-6541
Preprint. Discussion started: 12 February 2026

157 The surface WMF is transported upward level by level until reaching the model
158 top or critical level. At each model level, airflow instability is checked according to the
159 hypothesis of wave saturation (Lindzen, 1981) and wave-breaking (Miller and Palmer,
160 1986).

161 Once the subgrid-scale OGWs saturate and break, they will exert a body force
162 on the mean flow through the deposition of wave momentum, namely,

163 $$\frac{d\boldsymbol{V}(z)}{dt} = \frac{1}{\rho(z)}\frac{\partial \boldsymbol{\tau}(z)}{\partial z}. \quad (3)$$

164 where $\boldsymbol{V}(z)$ and $\boldsymbol{\tau}(z)$ are the mean flow velocity and the WMF at height z, respectively.
165 Note that both the directions of $\boldsymbol{V}(z)$ and $\boldsymbol{\tau}(z)$ are parallel to the mean flow at the low
166 level (i.e., $\boldsymbol{V_L}$). Readers are referred to KA95 for more details about the scheme.

167 The hydrostatic KA95 scheme above is revised by taking into account the NHE
168 on the surface WMF of OGWs, i.e.,

169 $$\tilde{\tau} = \tau_0[1 + NHE(Fr)]. \quad (4)$$

170 where the NHE correction depends only on the horizontal Froude number $Fr = \frac{|\boldsymbol{V_0}|}{N_0 L_x}$

171 $$NHE(Fr) = -\frac{9}{8}Fr^2 + e^{-2Fr^{-1}}\left(-\frac{5}{4}Fr^{-2} - \frac{1}{2}Fr^{-1} + \frac{5}{4} + \frac{9}{4}Fr + \frac{9}{8}Fr^2\right). \quad (5)$$

172 Note that the horizontal Froude number is different from the traditional Froude number
173 Fr_0 above which measures the flow nonlinearity. Moreover, Eq. (5) is the NHE derived
174 for three-dimensional isotropic terrain. While Xu et al. (2021) have derived the fully
175 NHE for anisotropic terrain, the expressions involve complicated integrals that are not
176 suitable for practical use in parameterization [cf. their Eqs. (14) to (17)]. Xu et al. (2021)
177 demonstrated that terrain anisotropy only has a very weak influence on the NHE, so the
178 expression of NHE for isotropic terrain, i.e., Eq. (5), is used because of simplicity, since

https://doi.org/10.5194/egusphere-2025-6541
Preprint. Discussion started: 12 February 2026

only algebraic manipulations are involved. This is in agreement with Xu et al. (2023, 2024) and Li et al. (2024).

b. Setup of numerical experiments

The CMA-GFSv4.0 dynamical core is based upon the nonhydrostatic and shallow atmospheric governing equations in spherical polar coordinates with full physics packages (Shen et al., 2020). It adopts a regular latitude-longitude grid of 0.125°× 0.125° with *C*-grid staggering. In the vertical, a terrain-following height-based grid is utilized along with Charney-Phillips staggering. There are 87 vertical levels, with the model top located at 73 km. For model physics, the Liu-Ma microphysics scheme (Ma et al., 2018) is employed, along with the RRTMG longwave and shortwave radiation schemes (Morcrette et al., 2008), the MRF planetary boundary layer scheme (Chen et al. 2020; Hong and Pan 1996), the CoLM land surface model (Dai et al., 2003), NSAS convection scheme (Han and Pan, 2011; Liu et al., 2015), the combined KA95 OGWD and LM97 FBD parameterization scheme (Chen et al., 2016), and Beljaars's TOFD scheme (Xue et al., 2011).

In order to examine the impact of the revised OGWD scheme on the medium-range forecast, two sets of numerical simulations (i.e., EXP_CTL and EXP_NHE) are conducted with different OGWD parameterization schemes, using the original KA95 scheme and the revised nonhydrostatic one, respectively. Both consist of 31 individual runs with their start dates from 00UTC 1 December to 00UTC 31 December in 2023. Herein, a winter month is chosen because the OGWD, which is mainly located in the Northern Hemisphere (NH) given the pronounced orography, is the strongest in this

https://doi.org/10.5194/egusphere-2025-6541
Preprint. Discussion started: 12 February 2026

season (e.g., Xu et al. 2020; Lu et al. 2024). In each experiment, the CMA-GFS model is integrated for 10 days, i.e., medium-range forecast, with 6-hr output interval. The model initial conditions are derived from the 0.25°×0.25° ECMWF Reanalysis v5 (ERA5) dataset (Hersbach et al., 2020), which are also used as reference for the evaluation of the CMA-GFS forecasts.

3. Evaluation of the medium-range forecast

a. Atmospheric circulation

Figure 1 shows the zonal-mean zonal wind averaged during the period of 10 December 2023 to 10 January 2024 (i.e., the 10th day of the medium-range forecast). In the winter of NH, as revealed by the ERA5 reanalysis (Fig. 1a), there is a subtropical jet in the midlatitudes troposphere, with the jet core located at about 200 hPa and 30°N. The maximum zonal wind speed exceeds 35 m s^{-1}. In the stratosphere of high latitudes, there is another wind maxima near 1 hPa and 60°N, which is the well-known polar-night jet (e.g., Kim, 2007). These two jets are separated around 70 hPa and 50°N, with the stratospheric jet being stronger than its tropospheric counterpart. In the Southern Hemisphere (SH), which is in summer, there is also a tropospheric jet but relatively weaker and lower than in the NH. The SH jet core is located at about 50°S, with a secondary one near 30°S. Given in the summer, the SH stratosphere is dominated by easterlies which is distinctly different from that in the NH. With a center located near 1 hPa and 20°S, the stratospheric easterlies extend downward and equatorward to the tropics. An easterly jet of over -30 m s^{-1} can be found near 20 hPa and 5°S.

https://doi.org/10.5194/egusphere-2025-6541
Preprint. Discussion started: 12 February 2026

Figure 1b is similar to Figure 1a but for the zonal-mean zonal winds obtained in the EXP_CTL experiment. In general, the CMA-GFS model can capture the overall pattern of the zonal-mean zonal winds, such as the tropospheric westerly jets in both hemispheres and the easterly winds in the SH stratosphere. The polar night jet in the NH, however, is underestimated by the model, with the jet core shifted southward by about 10 latitudes. As shown in Fig. 1c, there are notable easterly biases of over -5 m s^{-1} in the stratosphere of the NH high latitudes (north of 50°N). By contrast, westerly biases are present in the upper stratosphere of the NH midlatitudes (25°N-50°N) which can exceed 10 m s^{-1}, extending downward and equatorward to the lower stratosphere of the tropics. As in the NH troposphere, the zonal-mean zonal winds are overestimated in the Arctic region, but with easterly biases in the mid-lower latitudes. In the SH, the stratospheric easterlies are shifted northward, leading to westerly biases in the mid-lower latitudes (40°S-5°S) and easterly biases in the tropics and lower latitudes of the NH (5°S-20°N). In the high latitudes, there are predominantly easterly biases in both troposphere and stratosphere except in the upper stratosphere of the Antarctic region.

When taking into account the NHE in the OGWD parameterization scheme, the CMA-GFS model can better capture the large-scale circulation. Figure 1d presents the differences between the zonal-mean zonal winds in the two numerical experiments (i.e., EXP_NHE minus EXP_CTL). In the stratosphere above ~10 hPa, positive and negative wind differences are found to the north and south of 60°N, respectively, which are just opposed to the wind biases in Figure 1c. It suggests that both the magnitude and location of the polar night jet are improved. For example, the easterly biases in the mid-upper stratosphere (~10 hPa to 1 hPa) are reduced by about 3%. The westerly biases in the

https://doi.org/10.5194/egusphere-2025-6541
Preprint. Discussion started: 12 February 2026

247 troposphere of Arctica region are also reduced, which reaches up to about 42% of the
248 total bias.

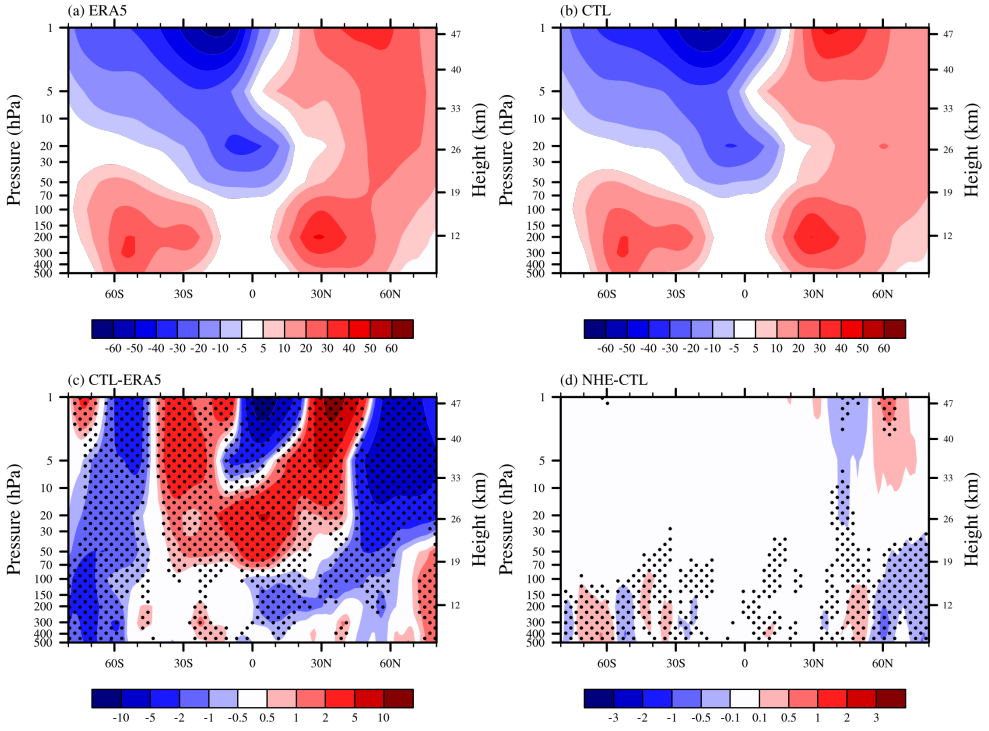

249

250 Figure 1. Vertical distributions of zonal-mean zonal wind (units: m s^{-1}) averaged in the
251 period of 10 December 2023 to 10 January 2024 obtained from (a) ERA5 and (b)
252 EXP_CTL, with their difference (i.e., EXP_CTL minus ERA5) given in (c). (d) is
253 similar to (c) but for the difference between the two experiments of EXP_NHE and
254 EXP_CTL (i.e., EXP_NHE minus EXP_CTL). Stippling in (c) and (d) denote
255 differences statistically significant at the 95% confidence level.
256

257 For the zonal-mean zonal wind biases in the SH stratosphere, they are hardly
258 alleviated, however. This is because the stratospheric OGWD is very weak in summer
259 (see Fig. 5a of Xu et al. 2024; see also Fig. 3 below), given the absorption of OGWs at
260 the critical level (Booker and Bretherton, 1967), that is, the zero-wind level between

https://doi.org/10.5194/egusphere-2025-6541
Preprint. Discussion started: 12 February 2026

261 the tropospheric westerlies and the stratospheric easterlies (Fig. 1a). The easterly biases
262 in the troposphere of the high latitudes are reduced, especially around 60°S.
263 Although there is no significant improvement for the zonal-mean zonal wind in
264 the NH mid-lower latitudes (Fig. 1d), the wind circulation can be improved regionally,
265 such as the East Asia subtropical jet (EASJ). Figure 2a shows the horizontal wind field
266 and speed at 200 hPa averaged in the period of 10 December 2023 to 10 January 2024
267 from the ERA5 reanalysis. In boreal winter, the EASJ stretches from about 110°E to
268 160°E in the latitudes between about 25°N and 45°N. The jet core is located near Japan,
269 showing a high wind speed of over 70 m s^{-1}. The simulated EASJ in the EXP_CTL
270 experiment generally aligns well with the ERA5 reanalysis, in terms of its location and
271 orientation (Fig. 2b). But the jet intensity is underestimated, showing easterly biases of
272 over -4 m s^{-1} (Fig. 2c). In the EXP_NHE experiment, the underestimation of the EASJ
273 is alleviated, with the mean bias decreased by about 6% (Fig. 2d).
274
275

https://doi.org/10.5194/egusphere-2025-6541
Preprint. Discussion started: 12 February 2026

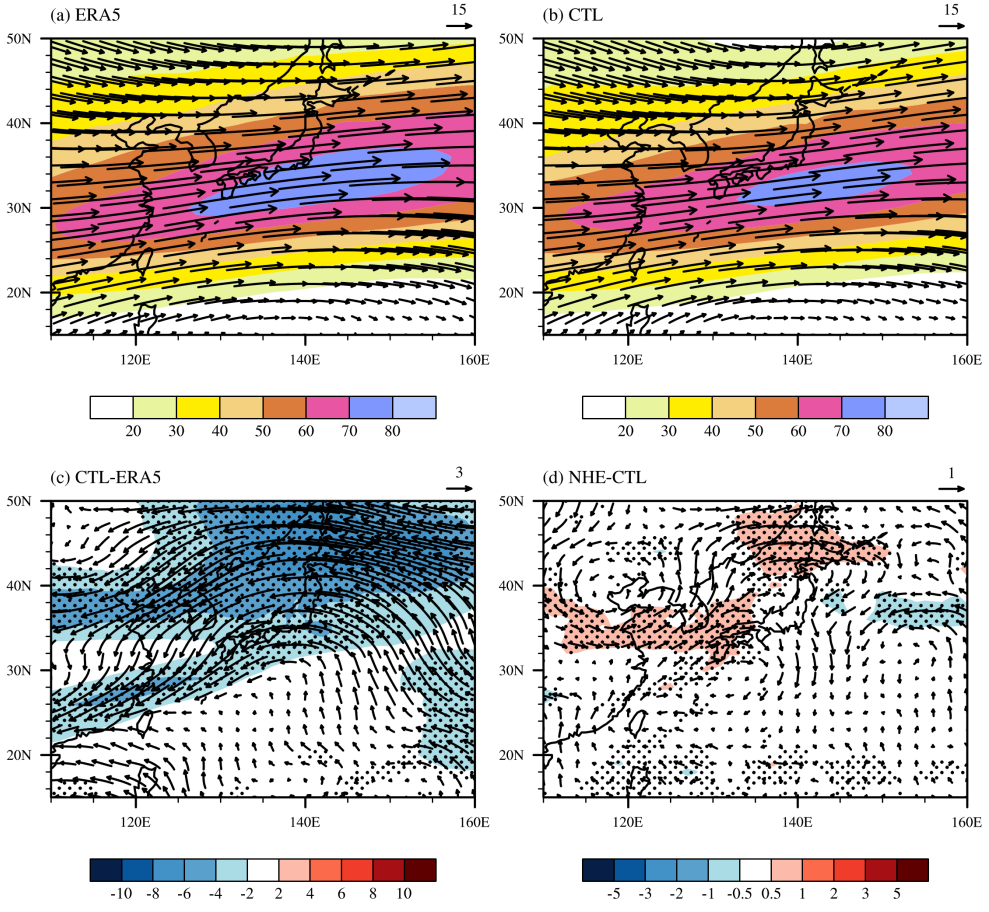

Figure 2. Horizontal distributions of wind speed (shading; units: m s^{-1}) and wind filed (arrow) at 200 hPa averaged in the period of 10 December 2023 to 10 January 2024 obtained from (a) ERA5 and (b) EXP_CTL, with their difference (i.e., EXP_CTL minus ERA5) given in (c). (d) is similar to (c) but for the difference between the two experiments of EXP_NHE and EXP_CTL (i.e., EXP_NHE minus EXP_CTL). Stippling in (c) and (d) denote differences statistically significant at the 95% confidence level.

b. Quantitative evaluation of forecast skills

For medium-range forecast, the wind circulation in the troposphere is often of greater interest than in the stratosphere. To better evaluate the performance of the

https://doi.org/10.5194/egusphere-2025-6541
Preprint. Discussion started: 12 February 2026

revised OGWD scheme, Figures 3a and 3b depict the mean bias (MB) and root mean square error (RMSE) for the 500 hPa geopotential height (GPH500) in the two experiments. Herein, we are interested in the NH because of the relatively weak wind differences in the SH (Fig. 1d) which is mainly covered by the ocean. Moreover, as will be shown below, the parameterized OGWD changes little in the SH.

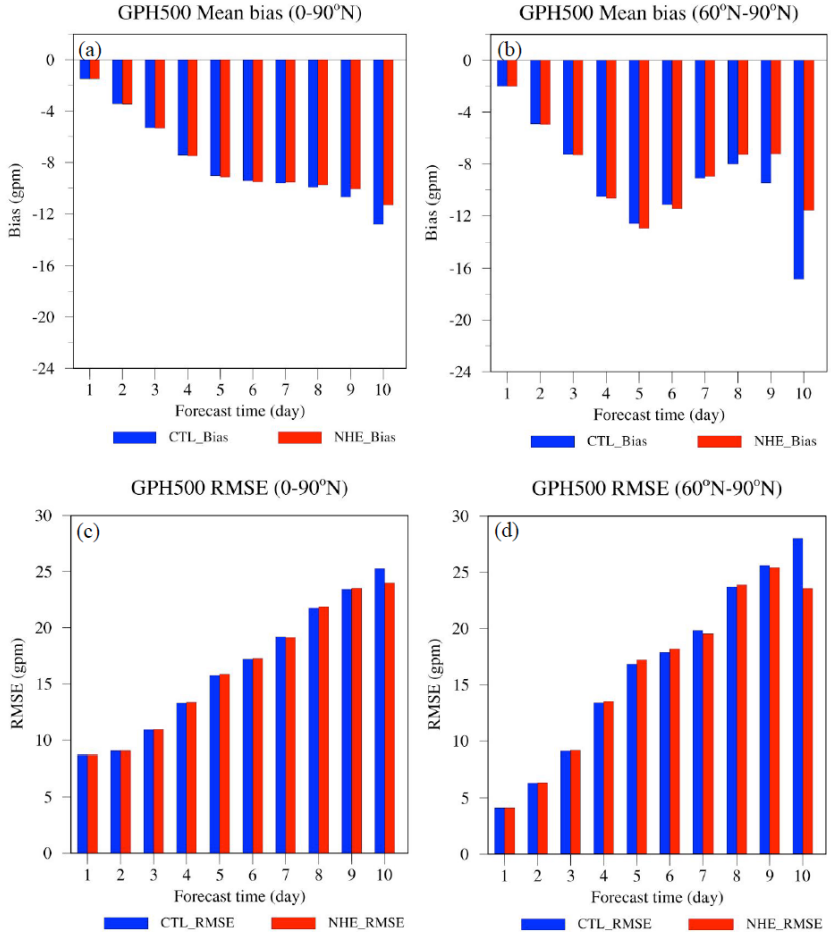

Figure 3. (a) Mean bias and (c) RMSE of the GPH500 in the NH at different forecast lead time. (b) and (d) are similar to (a) and (c) but in the region north of 60°N.

https://doi.org/10.5194/egusphere-2025-6541
Preprint. Discussion started: 12 February 2026

297 In both experiments, the model GPH500 is lower than the ERA5 reanalysis, with
298 the MB and RMSE increasing with the forecast lead time (Figs. 3a, 3c). The GPH500
299 shows obvious underestimation in the EXP_CTL experiment which are significantly
300 reduced in EXP_NHE. This improvement is particularly evident in high latitudes north
301 of 60°N which is overall statistically significant at the 95% confidence level (Figs. 4a,
302 4b). Compared to EXP_CTL, EXP_NHE exhibits even greater MB and RMSE of
303 GPH500 till the 6th forecast day. Nevertheless, both the MB and RMSE of the GPH500
304 decrease quickly afterwards, which are reduced by 11.59% and 5.06%, respectively, at
305 the 10th day of the forecast (Table 1). Greater improvements are found for the GPH500
306 between 60°N and 90°N, the MB and RMSE of which are decreased by 31.18% and
307 15.93%, respectively, at the 10th forecast day (Table 1). All the values shown in Table
308 1 are statistically significant at the 95% confidence level. For the total 10 forecast days
309 as a whole, the MB and RMSE of GPH500 are separately reduced by 2.6% and 0.52 %,
310 indicating an overall improvement in the simulation of the large-scale circulation in the
311 NH when using the revised OGWD scheme (see Table 2).

https://doi.org/10.5194/egusphere-2025-6541
Preprint. Discussion started: 12 February 2026

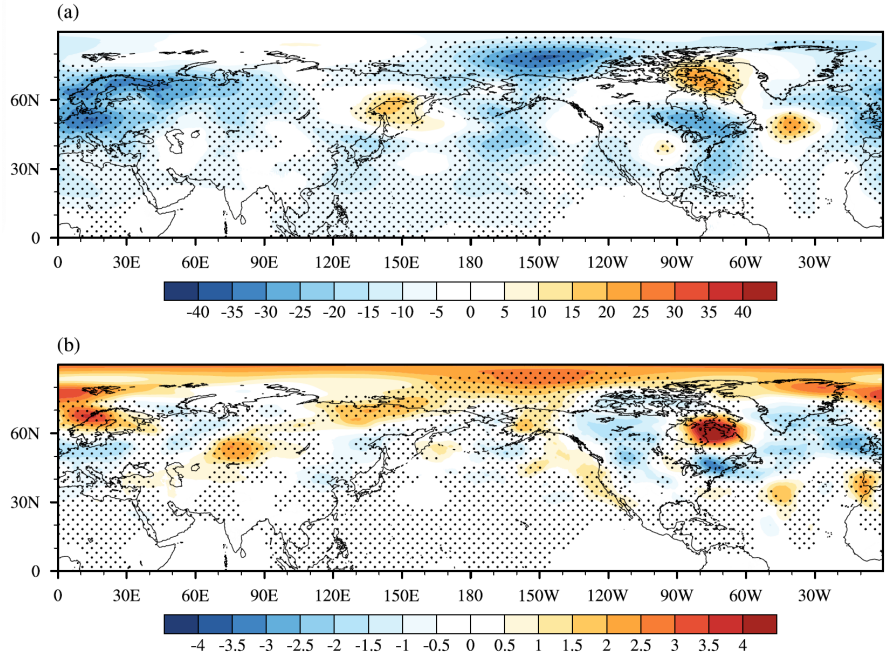

Figure 4. (a) Mean biases of GPH500 (shading; units: gpm) in EXP_CTL experiment as compared to ERA5 averaged over the ten forecast days. (b) is similar to (a) but for the differences between the GPH500 (shading; units: gpm) in EXP_CTL and EXP_NHE experiments (i.e., EXP_NHE minus EXP_CTL). Stippling in (a) and (b) denote differences statistically significant at the 95% confidence level.

Table 1. Mean bias and RMSE of the 500-hPa geopotential height (GPH500) and sea level pressure (SLP) at the 10th forecast day

		Mean Bias			RMSE		
	Region	CTL	NHE	$\frac{\text{NHE}-\text{CTL}}{CTL}\times 100$	CTL	NHE	$\frac{\text{NHE}-\text{CTL}}{CTL}\times 100$
GPH500 (gpm)	0-90°N	-12.825	-11.338	-11.59	25.263	23.984	-5.06
	60°N-90°N	-16.841	-11.590	-31.18	28.017	23.554	-15.93
SLP (hPa)	0-90°N	-0.522	-0.343	-34.29	2.714	2.515	-8.33
	60°N-90°N	-1.712	-1.079	-36.97	3.049	2.517	-17.45

https://doi.org/10.5194/egusphere-2025-6541
Preprint. Discussion started: 12 February 2026

Table 2. Mean bias and RMSE of the 500-hPa geopotential height (GPH500) and sea level pressure (SLP) for the overall ten forecast days

		Mean Bias			RMSE		
	Region	CTL	NHE	$\frac{\text{NHE}-\text{CTL}}{CTL}\times 100$	CTL	NHE	$\frac{\text{NHE}-\text{CTL}}{CTL}\times 100$
GPH500 (gpm)	0-90°N	-7.923	-7.717	-2.6	16.455	16.369	-0.52
	60°N-90°N	-9.187	-8.438	-8.15	16.470	16.089	-2.31
SLP (hPa)	0-90°N	-0.107	-0.082	-23.46	1.87	1.841	-1.53
	60°N-90°N	-0.498	-0.411	-17.47	1.598	1.532	-4.13

Besides the GPH500, the forecast skill is also examined for the SLP in the NH. As shown in Fig. 5a, the EXP_CTL experiment systematically underestimates the SLP over East Asia and the Arctic, while overestimating SLP across North America and the northern Atlantic. These biases are substantially corrected in the EXP_NHE experiment, particularly in high-latitude regions north of 60°N (Fig. 5b). Similarly, the EXP_NHE experiment firstly experiences a degradation in the early 6 days compared to EXP_CTL, but it shows significant improvement at the end of the 10th forecast day, with the MB reduced by 34.29% and the RMSE by 8.33%, respectively (Table 1). Greater decreases of 36.97% (for MB) and 17.45% (for RMSE) are found in the high latitudes north of 60°N as well.

https://doi.org/10.5194/egusphere-2025-6541
Preprint. Discussion started: 12 February 2026

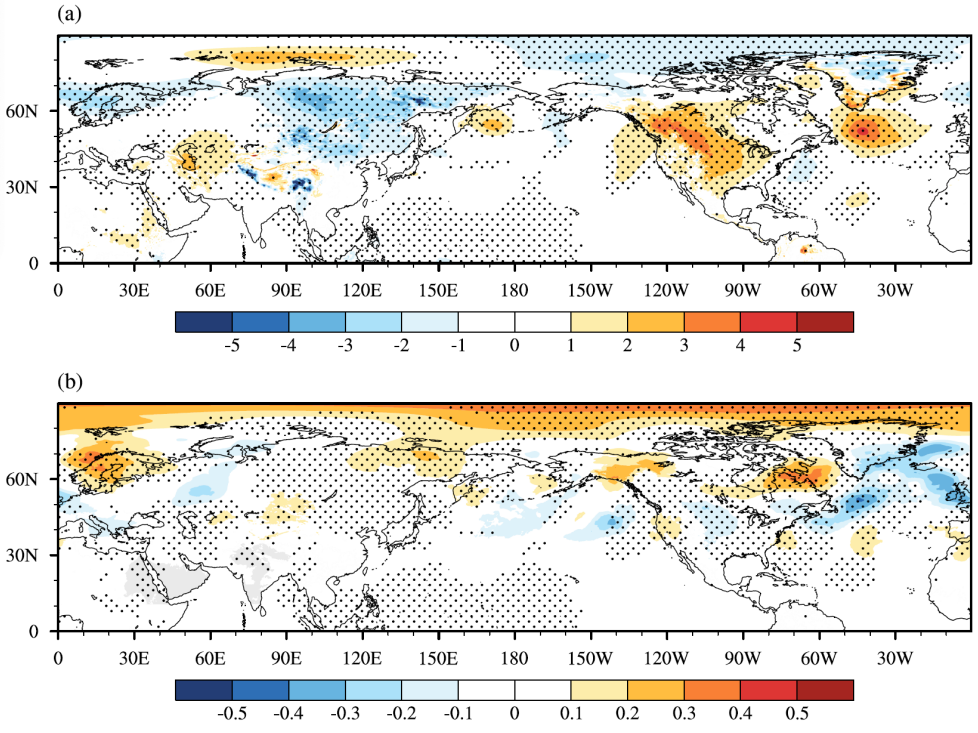

Figure 5. (a) Mean biases of SLP (shading; units: hPa) in the EXP_CTL experiment as compared to ERA5 averaged over the ten forecast days. (b) is similar to (a) but for the differences between the SLP (shading; units: hPa) in the EXP_CTL and EXP_NHE experiments (i.e., EXP_NHE minus EXP_CTL). Stippling in (a) and (b) denote differences statistically significant at the 95% confidence level.

From the above analyses, implementing the revised OGWD scheme in the high-resolution CMA-GFS model can help improve the medium range forecast of the NH large-scale circulation, especially in the high latitudes. In the next section, we will examine the underlying mechanisms responsible for the improvement of the circulation.

https://doi.org/10.5194/egusphere-2025-6541
Preprint. Discussion started: 12 February 2026

4. Physical interpretation

a. Changes of parameterized OGWD

The changes of wind circulation arise from the revision of the OGWD scheme. It is thus straightforward to study the parameterized OGWD in these two experiments. Figure 6a shows the vertical distribution of zonal-mean zonal OGWD averaged in the period of 10 December 2023 to 10 January 2024 in the EXP_CTL experiment. The differences between the parameterized OGWD in the two experiments (i.e., EXP_NHE minus EXP_CTL) are given in Fig. 6b. In boreal winter, there exists prominent OGWD in the stratosphere of the NH mid-to-high latitudes, which is favored by the decrease of air density with height (e.g., Lindzen, 1981) and the relatively weak winds between the tropospheric jet and polar night jet. The latter is called as the "valve layer" by Kruse et al. (2016). The maximum OGWD occurs between about 20 hPa and 1 hPa. In contrast, there is very weak OGWD in the SH stratosphere owing to the critical level absorption as mentioned above.

Compared to that in EXP_CTL, the zonal-mean zonal OGWD in EXP_NHE is generally weakened in the high latitudes of the NH (north of about 55°N), especially in the stratosphere (Fig. 6b). Note that the positive difference indicates a decrease of OGWD as the drag itself is negative. This is due to the fact that the NHE acts to decrease the surface WMF [see Eqs. (4) and (5)], i.e., the source of parameterized OGWs which determines the maximum wave momentum that can be deposited into the mean flow. Therefore, the decrease of surface WMF is prone to reduce the OGWD. Note that there is also enhancement of OGWD, e.g., in the stratosphere near 50°N. This is because the decrease of surface WMF may suppress wave breaking in the troposphere due to

https://doi.org/10.5194/egusphere-2025-6541
Preprint. Discussion started: 12 February 2026

reduced gravity wave amplitude. In consequence, more WMF is transported to the stratosphere where the OGWs break owing to the decay of air density and lead to stronger OGWD. This is similar to the redistribution of WMF in the vertical owing to selective critical level filtering of OGWs in directional shear flows (Shutts, 1995; Xu et al., 2012, 2019; van Niekerk et al., 2023). Generally, the changes in the vertical structure of parameterized OGWD in the CMA-GFS model are similar to that in the MPAS seasonal simulations conducted in Xu et al. (2024) which also considers the NHE correction to the OGWD (cf. their Fig. 5).

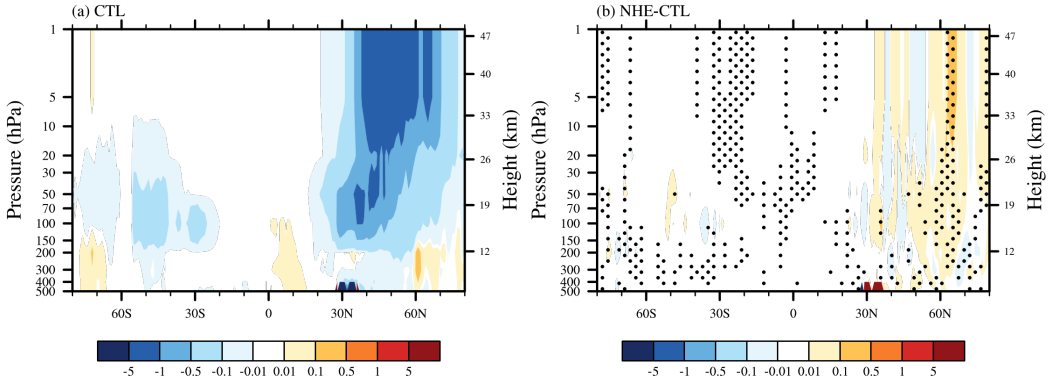

Figure 6. Vertical distributions of (a) zonal-mean zonal OGWD (units: m s^{-1} day^{-1}) averaged in the period of 10 December 2023 to 10 January 2024 obtained from EXP_CTL, and (b) zonal-mean OGWD difference between the two experiments of EXP_NHE and EXP_CTL (i.e., EXP_NHE minus EXP_CTL). Stippling in (b) denotes differences statistically significant at the 95% confidence level.

By the way, the parameterized OGWD in East Asia is also examined to explain the changes of EASJ. As shown in Fig. 7a, there is notable westward OGWD at 200 hPa in the high latitudes of East Asia where the underlying terrain is very complex,

https://doi.org/10.5194/egusphere-2025-6541
Preprint. Discussion started: 12 February 2026

such as the Taihang, Yanshan, Changbai, Greater Khingan and Lesser Khingan Mountains. Thus, the largest easterly biases of the EASJ occur in this region (Fig. 2c). When accounting for the NHE in the OGWD parameterization scheme, the 200-hPa OGWD is mainly reduced (Fig. 7b). Clearly, the enhanced EASJ is owing to the weakening of the parameterized OGWD.

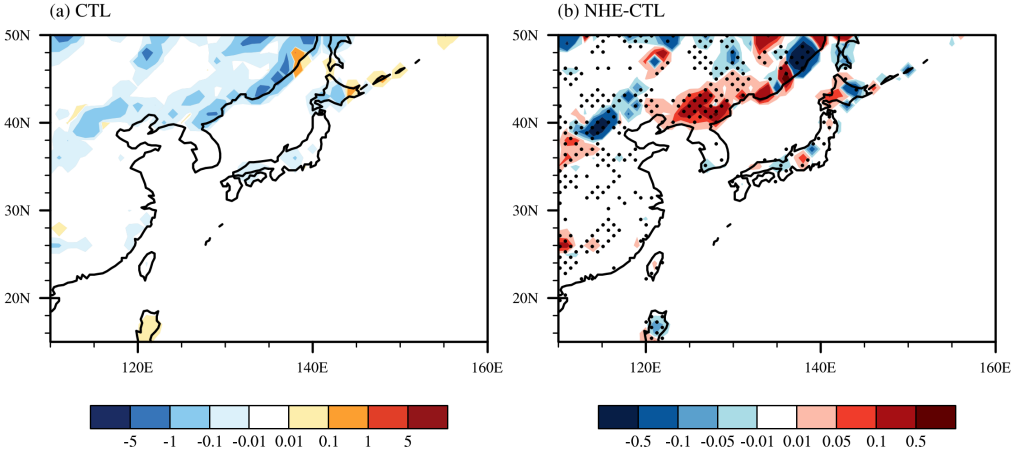

Figure 7. Horizontal distributions of (a) zonal OGWD (units: m s^{-1} day^{-1}) at 200 hPa averaged in the period of 10 December 2023 to 10 January 2024 obtained from EXP_CTL, and (b) zonal OGWD difference between the two experiments of EXP_NHE and EXP_CTL (i.e., EXP_NHE minus EXP_CTL) at 200 hPa. Stippling in (b) denotes differences statistically significant at the 95% confidence level.

b. Wave-induced secondary circulation: downward control mechanism

The weakening of stratospheric OGWD can directly increase the zonal wind in the polar stratosphere of the NH, thus leading to a recover of the weakened westerly jet (Figs. 1c, 1d). It can also affect the tropospheric circulation by inducing a secondary circulation according to the “downward control” principle (Haynes et al., 1991), i.e.,

https://doi.org/10.5194/egusphere-2025-6541
Preprint. Discussion started: 12 February 2026

$$\omega(p) = \frac{1}{r\partial\varphi}\left[\frac{1}{f}\int_0^p \bar{F}dp\right]. \quad (6)$$

where r is the radius of the earth, φ is the latitude, f is the Coriolis parameter, and ω is the vertical velocity in the pressure coordinate. The vertical velocity of the secondary circulation at a given pressure level is proportional to the meridional gradient of the vertically-integrated zonal wave forcing ($\bar{F}$) above this pressure level. Westward wave forcing ($\bar{F} < 0$) acts to induce ascending ($\omega < 0$) and sinking ($\omega > 0$) motions on the equatorward and poleward sides of the forcing, respectively. In contrast, the direction of the meridional circulation is reversed in the case of eastward wave forcing ($\bar{F} > 0$).

Figure 8 depicts the zonal-mean zonal OGWD in the mid-high latitudes of the NH which are vertically integrated from 200 hPa to the model top. In both experiments, the integrated zonal OGWD shows a decreasing trend from 50°N to 80°N. Compared to the EXP_CTL experiment, the EXP_NHE experiment produces an overall weaker westward OGWD between 50°N and 80°N, owing to the decrease of OGWD in the stratosphere (Fig. 6b). Therefore, the meridional gradient of the zonal OGWD is reduced, leading to greater upward motion poleward of about 70°N according to Eq. (6). In response to this upward motion, the NH polar stratosphere cools adiabatically, as can be seen clearly in Fig. 9. In contrast, the stratosphere warms adiabatically to the south of 60°N where the descending branch of the wave-induced secondary circulation exists. Given these temperature changes, the thermal contrast between the middle and high latitudes of the NH amplifies, which enhances the zonal wind in the stratosphere through the thermal wind relation for large-scale atmospheric motion.

https://doi.org/10.5194/egusphere-2025-6541
Preprint. Discussion started: 12 February 2026

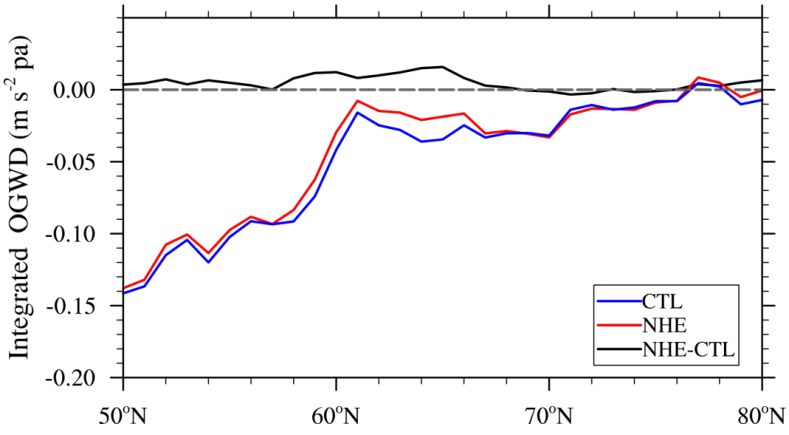

Figure 8. Zonal-mean zonal OGWD (units: m s^{-2} Pa) integrated above 200 hPa averaged in the period of 10 December 2023 to 10 January 2024 obtained from EXP_CTL (blue) and EXP_NHE (red), along with the difference between the two experiments of EXP_NHE and EXP_CTL (black).

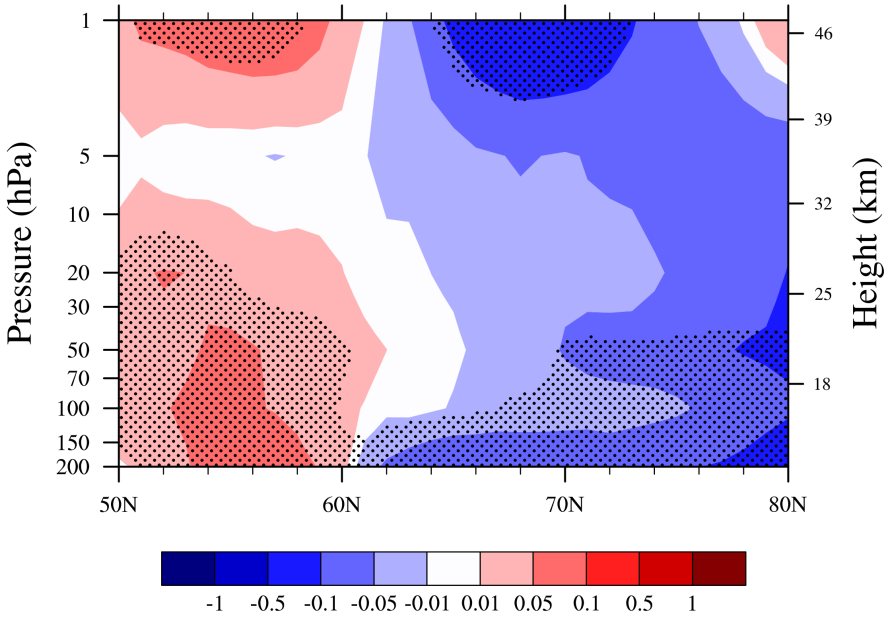

Figure 9. Vertical distribution of zonal-mean temperature difference between the two experiments of EXP_NHE and EXP_CTL (i.e., EXP_NHE minus EXP_CTL) averaged

https://doi.org/10.5194/egusphere-2025-6541
Preprint. Discussion started: 12 February 2026

in the period of 10 December 2023 to 10 January 2024 (units: K). Stippling denotes differences statistically significant at the 95% confidence level.

c. Role of Rossby waves: wave-mean flow interaction

While the polar stratospheric winds are increased, the polar tropospheric winds are weakened (Fig. 1d). The zonal OGWD in the troposphere does not change as notable as in the stratosphere (Fig. 6b). As shown below, the zonal-mean zonal winds in the polar troposphere are mainly influenced by the changes in resolved large-scale Rossby waves through the so-called catalytic wave-mean-flow positive feedback (White et al., 2021).

It is well known that the impacts of large-scale Rossby waves on the mean flow can be measured by the convergence of the zonal-mean Eliassen-Palm (EP) flux. Figure 10a illustrates the distribution of the zonal-mean EP flux in the EXP_CTL experiment which is calculated following Edmon et al. (1980). In the NH middle-to-high latitudes, Rossby waves originate from the lower troposphere which propagate upward and converge in the upper troposphere. These waves split into two branches in the lower stratosphere. The first branch turns to propagate equatorward across the tropospheric jet. The other branch continues to propagate upward to the upper stratosphere where the EP flux is converged and decelerates the mean flow. As in the SH, the Rossby waves cannot propagate into the stratosphere (not shown) because of the presence of easterlies there during austral summer (Fig. 1a).

Figure 10b is similar to Fig. 10a but gives the differences between the zonal-mean EP fluxes in the two experiments (i.e., EXP_NHE minus EXP_CTL). Compared to EXP_CTL, the upward propagation of Rossby waves into the stratosphere is

https://doi.org/10.5194/egusphere-2025-6541
Preprint. Discussion started: 12 February 2026

suppressed in the high latitudes of the NH, leading to an enhanced convergence of EP flux in the troposphere. As a result, the zonal-mean zonal winds in the NH polar troposphere are decelerated by the large-scale Rossby wave forcing, which contributes to the alleviation of westerly biases there (Fig. 1c, 1d). This may explain why the improvements in the GPH 500 forecast emerge after 6 days in EXP_NHE (Fig. 2). The Rossby waves and their interaction with the mean flow require several days to develop fully and influence the large-scale circulation.

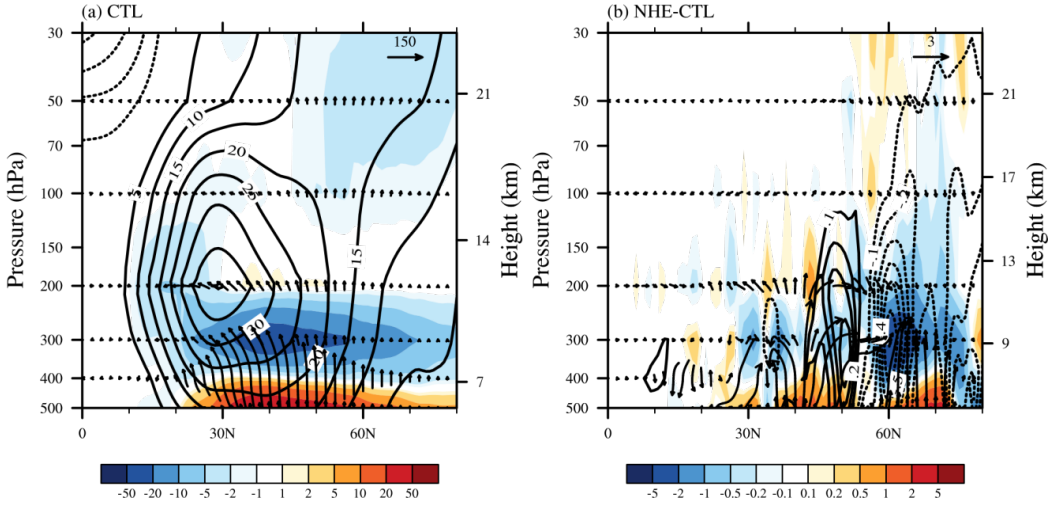

Figure 10. Vertical distributions of zonal-mean EP flux (vectors) and its divergence (shading; m s^{-1} day^{-1}) due to resolved waves averaged in the period of 10 December 2023 to 10 January 2024 obtained from (a) EXP_CTL, and (b) the difference between the two experiments of EXP_NHE and EXP_CTL (i.e., EXP_NHE minus EXP_CTL). Contours are the corresponding zonal-mean zonal wind (units: m s^{-1}).

The suppressed upward propagation of Rossby waves can be understood from the changes of the refractive index (*RFI*) that measures the ability of Rossby wave propagation (e.g., Chen and Robinson, 1992; Hu et al., 2019), which is defined as

https://doi.org/10.5194/egusphere-2025-6541
Preprint. Discussion started: 12 February 2026

$$RFI = \left[\frac{\overline{q_\varphi}}{r\bar{U}} - \left(\frac{k}{rcos\varphi}\right)^2 - \left(\frac{f}{2NH}\right)^2\right] r^2 , \quad (7)$$

where $\bar{U}$, k and H are the resolved zonal-mean zonal wind, zonal wave number and density scale height, respectively. $\overline{q_\varphi}$ represents the meridional gradient of the potential vorticity, which is expressed in the following form of

$$\overline{q_\varphi} = 2\Omega\cos\varphi - \left[\frac{(\bar{U}cos\varphi)_\varphi}{acos\varphi}\right]_\varphi + \frac{af^2}{R_d}\left(\frac{p\theta}{T}\frac{\overline{U_p}}{\overline{\theta_p}}\right)_p . \quad (8)$$

where Ω, θ and R_d being the Earth's angular frequency, potential temperature and dry gas constant, respectively. The subscripts φ and p represent the partial derivatives with respect to latitude and pressure, respectively. The overbars indicate temporal and zonal averages. From Eq. (7), the increase of zonal wind will narrow the range of Rossby wave numbers that can propagate into the stratosphere (Charney and Drazin, 1961; Xu et al., 2024). As analyzed above, the weekend OGWD in the polar stratosphere enhances the zonal winds there, thus inhabiting the upward propagation of Rossby waves.

4. Summary and discussions

The latest China Meteorological Administration Global Forecast System (CMA-GFS) v4.0 model has been upgraded to a higher resolution of 0.125° in 2023. However, this high-resolution global model still uses the parameterization scheme of orographic gravity wave drag (OGWD) developed by Kim and Arakawa (1995; KA95) which is based on hydrostatic orographic gravity wave (OGW) theory. In this study, the KA95 OGWD scheme is revised by taking into account the nonhydrostatic effect (NHE) on the surface wave momentum flux (WMF) of OGWs, according to the nonhydrostatic

https://doi.org/10.5194/egusphere-2025-6541
Preprint. Discussion started: 12 February 2026

OGW theory derived in our earlier study of Xu et al. (2021). The performance of the revised OGWD scheme is then evaluated for the medium-range forecast of the CMA-GFSv4.0 model. Two sets of numerical experiments (i.e., EXP_CTL and EXP_NHE) are conducted by using the original KA95 scheme and the revised NHE scheme, respectively. In each numerical experiment, there are in total 31 forecasts of 10-day forecasts which are initiated at 0000 UTC of each day in December 2023.

The results show that the revised OGWD scheme can improve the medium-range forecast of large-scale circulation in the Northern Hemisphere (NH), especially in the high latitudes. The easterly biases of zonal-mean zonal wind in the NH stratosphere are reduced, with both the magnitude and location of the polar night jet being better captured. The underestimation of the East Asia subtropical jet (EASJ) is also alleviated. In contrast, the revised OGWD scheme shows little influence on the stratospheric circulation in the Southern Hemisphere (SH). This is because, in boreal winter (i.e., austral summer), there is hardly OGWD in the SH stratosphere owing to the effect of critical-level absorption.

Quantitative evaluation is performed for the medium-range forecast skills in the NH, taking the ERA5 reanalysis dataset as reference. Both experiments showed lower geopotential height (GPH) at 500 hPa than ERA5 reanalysis, with the mean bias (MB) and root mean square error (RMSE) increasing with forecast lead time. EXP_NHE initially has greater MB and RMSE than EXP_CTL until the 6th forecast day, but these metrics decrease more rapidly afterwards, resulting in an 11.59% reduction in MB and a 5.06% reduction in RMSE by day 10. Over the total 10 forecast days, the MB and RMSE of the GPH 500 in the NH are reduced by 2.6% and 0.52%, respectively,

https://doi.org/10.5194/egusphere-2025-6541
Preprint. Discussion started: 12 February 2026

525 indicating improved simulation of large-scale circulation in the NH. The improvement
526 is more noticeable in the high latitudes north of about 60°N, where the MB and RMSE
527 of GPH 500 are decreased by 31.18% and 15.93% at the 10th forecast day. Similar
528 results are found for the sea level pressure (SLP) in the NH, the MB and RMSE of
529 which are reduced by 34.29% and 8.33%, respectively, by day 10 in EXP_NHE.

530 The dynamics responsible for the improvement of large-scale wind circulation are
531 examined. The NHEs act to decrease the surface WMF of OGWs, which leads to a general
532 weakening of the parameterized OGWD in the high latitudes of the NH, especially in the
533 stratosphere. This weakening of stratospheric OGWD directly increases the zonal wind in
534 the polar stratosphere, reducing the easterly biases. It also induces a secondary circulation
535 according to the "downward control" principle, causing adiabatic cooling in the NH polar
536 stratosphere and warming to the south of 60°N. The resultant increase in thermal contrast
537 between the middle and high latitudes enhances the zonal wind in the stratosphere through
538 the thermal wind relation. The enhanced zonal wind in the polar stratosphere acts to narrow
539 the range of large-scale Rossby wave numbers that can propagate into the stratosphere
540 by reducing the refractive index of Rossby waves. The suppressed upward propagation of
541 Rossby waves leads to greater convergence of Eliassen-Palm (EP) flux (i.e., resolved wave
542 forcing) in the NH polar troposphere, which decelerates the zonal winds and thus alleviates
543 the westerly biases there.

544 To sum up, this study demonstrates that incorporating the NHE into the OGWD
545 parameterization scheme can help improve the simulation of large-scale atmospheric
546 circulation in high-resolution global NWP models, which is thus important for accurate
547 weather forecasts and/or climate simulations. However, there are still some limitations in

https://doi.org/10.5194/egusphere-2025-6541
Preprint. Discussion started: 12 February 2026

this work. For example, this study pays much attention to the medium-range forecast of large-scale circulation in winter of NH. To further validate its effectiveness and robustness, it is necessary to conduct more comprehensive evaluations of the nonhydrostatic OGWD scheme in various numerical models focusing on different weather and climate systems. Additionally, this work only takes into account the effects of NHE on the OGWD. Other factors such as the vertical wind shear could also greatly affect the OGWD (e.g., Xu et al., 2019; Xu et al., 2020; Zhang et al., 2025). While Xu et al. (2021) explored the nonhydrostatic OGWs generated in a constant flow, it remains unclear how the vertical wind shear affects the behavior of nonhydrostatic OGWs which needs further study.

Code and data availability. The China Meteorological Administration Global Forecast System (CMA-GFS) model is archived on Zenodo under https://doi.org/10.5281/zenodo.18476721 (Zhang, 2026). The CMA-GFS outputs and the ERA5 reanalysis data used for the comparison, along with the codes for orographic gravity wave scheme are uploaded to https://doi.org/10.5281/zenodo.18529537 (Zhang, 2026).

Author contributions. RRZ was responsible for formal analysis, writing the original draft and visualization. ZZA carried out data analyses. XX developed the code and conducted the analysis. HLX and QYC provided the resources and data curation.

Competing interests. The contact author has declared that none of the authors has any competing interests.

https://doi.org/10.5194/egusphere-2025-6541
Preprint. Discussion started: 12 February 2026

Acknowledgements. The authors would like to express their sincere thanks to the anonymous referees.

Financial support. This work is mainly supported by the National Natural Science Foundation of China (grants no. U2342226, 42275163), the Joint Research Project for Meteorological Capacity Improvement (grant no. 22NLTSZ006), and Jiangsu Meteorological Observatory (grant no. KQ202502).

https://doi.org/10.5194/egusphere-2025-6541
Preprint. Discussion started: 12 February 2026

References

Alexander, M. J., Geller, M., McLandress, C., Polavarapu, S., Preusse, P., Sassi, F., Sato, K., Eckermann, S., Ern, M., Hertzog, A., Kawatani, Y., Pulido, M., Shaw, T.A., Sigmond, M., Vincent, R. and Watanabe, S.: Recent developments in gravity-wave effects in climate models and the global distribution of gravity-wave momentum flux from observations and models, Quarterly Journal of the Royal Meteorological Society, 136, 1103-1124, https://doi.org/10.1002/qj.637, 2010.

Alpert, J.: Sub-grid scale mountain blocking at NCEP, 20th Conference on Weather Analysis and Forecasting/16th Conference on Numerical Weather Prediction, https://ams.confex.com/ams/84Annual/techprogram/program_185.htm, 2004.

Beljaars, A. C. M., Brown, A. R., and Wood, N.: A new parametrization of turbulent orographic form drag, Quarterly Journal of the Royal Meteorological Society, 130, 1327-1347, https://doi.org/10.1256/qj.03.73, 2004.

Booker, J. R., and Bretherton, F. P.: The critical layer for internal gravity waves in a shear flow, Journal of Fluid Mechanics, 27, 513-539, https://doi.org/10.1017/S0022112067000515, 1967.

Charney, J. G., and Drazin, P. G.: Propagation of planetary-scale disturbances from the lower into the upper atmosphere, Journal of Geophysical Research (1896-1977), 66, 83-109, https://doi.org/10.1029/JZ066i001p00083, 1961.

Chen, J., Ma, Z., Li, Z., Shen, X., Su, Y., Chen, Q., and Liu, Y.: Vertical diffusion and cloud scheme coupling to the Charney-Phillips vertical grid in GRAPES global forecast system, Quarterly Journal of the Royal Meteorological Society, 146, 2191-2204, https://doi.org/10.1002/qj.3787, 2020.

https://doi.org/10.5194/egusphere-2025-6541
Preprint. Discussion started: 12 February 2026

603 Chen Q., Shen, X., Sun, J., and Liu, K.: Momentum budget diagnosis and the
604 parameterization of subgrid-scale orographic drag in global GRAPES, Journal of
605 Meteorological Research, 30, 771-788, https://doi.org/10.1007/s13351-016-6033-
606 y, 2016.
607 Chen, P., and Robinson, W. A.: Propagation of Planetary Waves between the Troposphere
608 and Stratosphere, Journal of Atmospheric Sciences, 49, 2533-2545,
609 https://doi.org/10.1175/1520-0469(1992)049<2533:POPWBT>2.0.CO;2, 1992.
610 Choi, H. J., and Hong, S. Y.: An updated subgrid orographic parameterization for global
611 atmospheric forecast models, Journal of Geophysical Research: Atmospheres, 120,
612 12445-12457, https://doi.org/10.1002/2015JD024230, 2015.
613 Dai, Y., Zeng, X., Robert, E. D., Baker, L., Bonan, G. B., Bosilovich, M. G., Denning A.
614 S., Dirmeyer, P. A., Houser, P. R., Niu, G., Oleson, K. W., Schlosser, C. A., Yang,
615 Z.: The Common Land Model, Bulletin of the American Meteorological Society,
616 84, 1013-1024, https://doi.org/10.1175/BAMS-84-8-1013, 2003.
617 Edmon, H. J., Hoskins, B. J. and McIntyre, M. E.: Eliassen-Palm Cross Sections for the
618 Troposphere, Journal of Atmospheric Sciences, 37, 2600-2616,
619 https://doi.org/10.1175/1520-0469(1980)037<2600:EPCSFT>2.0.CO;2, 1980.
620 Fritts, D. C., and Alexander, M. J.: Gravity wave dynamics and effects in the middle
621 atmosphere, Reviews of Geophysics, 41, https://doi.org/10.1029/2001RG000106,
622 2003.
623 Han, J., and Pan, H. L.: Revision of Convection and Vertical Diffusion Schemes in the
624 NCEP Global Forecast System, Weather and Forecasting, 26, 520-533,
625 https://doi.org/10.1175/WAF-D-10-05038.1, 2011.

https://doi.org/10.5194/egusphere-2025-6541
Preprint. Discussion started: 12 February 2026

626 Haynes, P. H., Mclntyre, M. E., Shepherd, T. G., Marks, C. J., and Shine, K. P.: On the
627 "Downward Control" of Extratropical Diabatic Circulations by Eddy-Induced
628 Mean Zonal Forces, Journal of Atmospheric Sciences, 48, 651-678,
629 https://doi.org/10.1175/1520-0469(1991)048<0651:OTCOED>2.0.CO;2, 1991.
630 Hersbach, H., Bell, B., Berrisford, P., et al: The ERA5 global reanalysis, Quarterly Journal
631 of the Royal Meteorological Society, 146, 1999-2049,
632 https://doi.org/10.1002/qj.3803, 2020.
633 Hong, S. Y., and Pan, H. L.: Nonlocal Boundary Layer Vertical Diffusion in a Medium-
634 Range Forecast Model, Monthly Weather Review, 124, 2322-2339,
635 https://doi.org/10.1175/1520-0493(1996)124<2322:NBLVDI>2.0.CO;2, 1996.
636 Hu, D., Guo, Y., and Guan, Z.: Recent Weakening in the Stratospheric Planetary Wave
637 Intensity in Early Winter, Geophysical Research Letters, 46, 3953-3962,
638 https://doi.org/10.1029/2019GL082113, 2019.
639 Kim, Y. J.: Balance of drag between the middle and lower atmospheres in a global
640 atmospheric forecast model, Journal of Geophysical Research: Atmospheres, 112,
641 https://doi.org/10.1029/2007JD008647, 2007.
642 Kim, Y. J., and Arakawa, A.: Improvement of Orographic Gravity Wave Parameterization
643 Using a Mesoscale Gravity Wave Model, Journal of Atmospheric Sciences, 52,
644 1875-1902, https://doi.org/10.1175/1520-
645 0469(1995)052<1875:IOOGWP>2.0.CO;2, 1995.
646 Kim, Y. J., and Doyle, J. D.: Extension of an orographic-drag parametrization scheme to
647 incorporate orographic anisotropy and flow blocking, Quarterly Journal of the

https://doi.org/10.5194/egusphere-2025-6541
Preprint. Discussion started: 12 February 2026

Royal Meteorological Society, 131, 1893-1921, https://doi.org/10.1256/qj.04.160, 2005.

Kim, Y. J., Eckermann, S., and Chun, H. Y.: An overview of the past, present and future of gravity-wave drag parametrization for numerical climate and weather prediction models - Survey article, Atmosphere-ocean, 41, 65-98, https://doi.org/10.3137/ao.410105, 2003.

Klemp, J. B., and Durran, D. R.: An Upper Boundary Condition Permitting Internal Gravity Wave Radiation in Numerical Mesoscale Models, Monthly Weather Review, 111, 430-444, https://doi.org/10.1175/1520-0493(1983)111<0430:AUBCPI>2.0.CO;2, 1983.

Kruse, C. G., Smith, R. B., and Eckermann, S. D.: The Midlatitude Lower-Stratospheric Mountain Wave "Valve Layer", Journal of the Atmospheric Sciences, 73, 5081-5100, https://doi.org/10.1175/JAS-D-16-0173.1, 2016.

Li, M., Xu, X., Teixeira, M. A. C., Xue, M., Xue, H., Zhu, K., and Huang, H.: Improved Orographic Gravity Wave Drag Parameterization Accounting for the Nonhydrostatic Effect in the Weather Research and Forecasting Model: Tests for Short-Range Forecast of Northeast China Cold Vortices, Monthly Weather Review, 152, 2623-2637, https://doi.org/10.1175/MWR-D-24-0097.1, 2024.

Li, R., Xu, X., Xu, X., Shepherd, T. G., and Wang, Y.: Importance of orographic gravity waves over the Tibetan Plateau on the spring rainfall in East Asia, Science China Earth Sciences, 66, 2594-2602, https://doi.org/10.1007/s11430-023-1204-6, 2023.

https://doi.org/10.5194/egusphere-2025-6541
Preprint. Discussion started: 12 February 2026

669 Lindzen, R. S.: Turbulence and stress owing to gravity wave and tidal breakdown, Journal
670 of Geophysical Research: Oceans, 86, 9707-9714,
671 https://doi.org/10.1029/JC086iC10p09707, 1981.
672 Liu, K., Chen, Q., and Sun, J.: Modification of cumulus convection and planetary boundary
673 layer schemes in the GRAPES global model, Journal of Meteorological Research,
674 29, 806-822, https://doi.org/10.1007/s13351-015-5043-5, 2015.
675 Lott, F., and Miller, M. J.: A new subgrid-scale orographic drag parametrization: Its
676 formulation and testing, Quarterly Journal of the Royal Meteorological Society,
677 123, 101-127, https://doi.org/10.1002/qj.49712353704, 1997.
678 Lu, Y., Wu, T., Xu, X., Zhang, L., and Chu, M.: Improved Simulation of the Antarctic
679 Stratospheric Final Warming by Modifying the Orographic Gravity Wave
680 Parameterization in the Beijing Climate Center Atmospheric General Circulation
681 Model, Atmosphere, 11, 576, https://doi.org/10.3390/atmos11060576, 2020.
682 Lu, Y., Xu, X., Wang, L., Liu, Y., Wu, T., Jie, W., and Sun, J.: Machine Learning
683 Emulation of Subgrid-Scale Orographic Gravity Wave Drag in a General
684 Circulation Model with Middle Atmosphere Extension, J. Adv. Model. Earth Syst.,
685 16, e2023MS003611, https://doi.org/10.1029/2023MS003611, 2024.
686 Ma, Z., Liu, Q., Zhao, C., Shen, X., Wang, Y., Jiang, J. H., Zhe, L., and Yung, Y.:
687 Application and Evaluation of an Explicit Prognostic Cloud-Cover Scheme in
688 GRAPES Global Forecast System, Journal of Advances in Modeling Earth Systems,
689 10, 652-667, https://doi.org/10.1002/2017MS001234, 2018.
690 McFarlane, N. A.: The Effect of Orographically Excited Gravity Wave Drag on the General
691 Circulation of the Lower Stratosphere and Troposphere, Journal of Atmospheric

https://doi.org/10.5194/egusphere-2025-6541
Preprint. Discussion started: 12 February 2026

692 Sciences, 44, 1775-1800, https://doi.org/10.1175/1520-
693 0469(1987)044<1775:TEOOEG>2.0.CO;2, 1987.
694 McLandress, C., Shepherd, T. G., Polavarapu, S., and Beagley, S. R.: Is Missing
695 Orographic Gravity Wave Drag near 60°S the Cause of the Stratospheric Zonal
696 Wind Biases in Chemistry-Climate Models? Journal of the Atmospheric Sciences,
697 69, 802-818, https://doi.org/10.1175/JAS-D-11-0159.1, 2012.
698 Miller, M. J., and Palmer, T. N.: Orographic gravity wave drag: Its parameterization and
699 influence in general circulation and numerical weather prediction models,
700 Presented at the ECWMF Workshop on Observation, Theory and Modelling of
701 Orographic Effects 1, 283-333, 1986.
702 Morcrette, J. J., Barker, H. W. J., Cole, N. S., Iacono, M. J., and Pincus, R.: Impact of a
703 New Radiation Package, McRad, in the ECMWF Integrated Forecasting System,
704 Monthly Weather Review, 136, 4773-4798,
705 https://doi.org/10.1175/2008MWR2363.1, 2008.
706 Palmer, T. N., Shutts, G. J., and Swinbank, R.: Alleviation of a systematic westerly bias in
707 general circulation and numerical weather prediction models through an orographic
708 gravity wave drag parametrization, Quarterly Journal of the Royal Meteorological
709 Society, 112, 1001-1039, https://doi.org/10.1002/qj.49711247406, 1986.
710 Scinocca, J., and McFarlane, N.: The parametrization of drag induced by stratified flow
711 over anisotropic orography, Quarterly Journal of the Royal Meteorological Society,
712 126, 2353-2393, https://doi.org/10.1002/qj.49712656802, 2000.

https://doi.org/10.5194/egusphere-2025-6541
Preprint. Discussion started: 12 February 2026

713 Shen, X., Su, Y., Hu, J., et al.: Development and Operation Transformation of GRAPES
714 Global Middle-range Forecast System, Journal of Applied Meteorological Science,
715 28, 1-10, https://doi.org/10.11898/1001-7313.20170101, 2017.
716 Shen, X., Wang, J., Li, Z., Chen, D., and Gong, J.: Research and operational development
717 of numerical weather prediction in China, Journal of Meteorological Research, 34,
718 675-698, https://doi.org/10.1007/s13351-020-9847-6, 2020.
719 Shutts, G.: Gravity-wave drag parametrization over complex terrain: The effect of critical-
720 level absorption in directional wind-shear, Quarterly Journal of the Royal
721 Meteorological Society, 121, 1005-1021, https://doi.org/10.1002/qj.49712152504,
722 1995.
723 Smith, R. B.: The Influence of Mountains on the Atmosphere, In B. Saltzman (Ed.),
724 Advances in Geophysics (Vol. 21, pp. 87-230): Elsevier, 1979.
725 Teixeira, M. A. C.: The physics of orographic gravity wave drag, Frontiers in Physics, 2,
726 https://doi.org/10.3389/fphy.2014.00043, 2014.
727 van Niekerk, A., Vosper, S. B., and Teixeira, M. A. C.: Accounting for the three-
728 dimensional nature of mountain waves: Parametrising partial critical-level filtering,
729 Quarterly Journal of the Royal Meteorological Society, 149, 515-536,
730 https://doi.org/10.1002/qj.4421, 2023.
731 Wei, P., Xu, X., Xue, M., Li, J., Zhao, K., and Zhang, Q.: Complex Terrain Causes Global
732 Model Prediction Biases of 21.7 Zhengzhou Extreme Precipitation, Science
733 Bulletin, https://doi.org/10.1016/j.scib.2025.09.015, 2025.

https://doi.org/10.5194/egusphere-2025-6541
Preprint. Discussion started: 12 February 2026

734 White, R. H., Wallace, J. M., and Battisti, D. S.: Revisiting the Role of Mountains in the
735 Northern Hemisphere Winter Atmospheric Circulation, Journal of the Atmospheric
736 Sciences, 78, 2221-2235, https://doi.org/10.1175/JAS-D-20-0300.1, 2021.
737 Xu, X., Zhou, X., Yang, K., Lu, Y., Zhang, R., Yang, B., Tang, J., Wang, Y.: Reducing
738 Winter Precipitation Biases Over the Western Tibetan Plateau in the Model for
739 Prediction Across Scales (MPAS) With a Revised Parameterization of Orographic
740 Gravity Wave Drag, Journal of Geophysical Research: Atmospheres, 128,
741 e2023JD039123, https://doi.org/10.1029/2023JD039123, 2023.
742 Xu, X., Li, R., Teixeira, M. A. C., and Lu, Y.: On the Momentum Flux of Vertically
743 Propagating Orographic Gravity Waves Excited in Nonhydrostatic Flow over
744 Three-Dimensional Orography, Journal of the Atmospheric Sciences, 78, 1807-
745 1822, https://doi.org/10.1175/JAS-D-20-0370.1, 2021.
746 Xu, X., Teixeira, M. A. C., Xue, M., Lu, Y., and Tang, J.: Impacts of wind profile shear
747 and curvature on the parameterized orographic gravity wave stress in the Weather
748 Research and Forecasting model, Quarterly Journal of the Royal Meteorological
749 Society, 146, 3086-3100, https://doi.org/10.1002/qj.3828, 2020.
750 Xu, X., Wang, Y., and Xue, M.: Momentum Flux and Flux Divergence of Gravity Waves
751 in Directional Shear Flows over Three-Dimensional Mountains, Journal of the
752 Atmospheric Sciences, 69, 3733-3744, https://doi.org/10.1175/JAS-D-12-044.1,
753 2012.
754 Xu, X., Xue, M., Teixeira, M. A. C., Tang, J., and Wang, Y.: Parameterization of
755 Directional Absorption of Orographic Gravity Waves and Its Impact on the
756 Atmospheric General Circulation Simulated by the Weather Research and

https://doi.org/10.5194/egusphere-2025-6541
Preprint. Discussion started: 12 February 2026

Forecasting Model, Journal of the Atmospheric Sciences, 76, 3435-3453, https://doi.org/10.1175/JAS-D-18-0365.1, 2019.

Xu, X., Zhang, R., Teixeira, M. A. C., van Niekerk, A., Xue, M., Lu, Y., Xue, H., Li, R., Wang, Y.: A Parameterization Scheme Accounting for Nonhydrostatic Effects on the Momentum Flux of Vertically Propagating Orographic Gravity Waves: Formulas and Preliminary Tests in the Model for Prediction Across Scales (MPAS), Journal of the Atmospheric Sciences, 81, 805-817, https://doi.org/10.1175/JAS-D-23-0020.1, 2024.

Xue, H., Shen, X., and Su, Y.: Parameterization of Turbulent Orographic Form Drag and Implementation in GRAPES, Journal of Applied Meteorological Science, 22, 169-181, http://qikan.camscma.cn/en/article/id/20110206, 2011.

Zängl, G.: Orographic Gravity Waves Close to the Nonhydrostatic Limit of Vertical Propagation, Journal of the Atmospheric Sciences, 60, 2045-2063, https://doi.org/10.1175/1520-0469(2003)060<2045:OGWCTT>2.0.CO;2, 2003.

Zhang, R.: CMA-GFS Model. Zenodo [code], https://doi.org/10.5281/zenodo.18476721, 2026.

Zhang, R.: CMA-GFS outputs. Zenodo [data set], https://doi.org/10.5281/zenodo.18529537, 2026.

Zhang, R., Lu, Y., Xu, X., and Wang, Y.: Impacts of wind profile shear and curvature on the parameterized orographic gravity wave stress in a middle atmosphere resolving general circulation model, Journal of Advances in Modeling Earth Systems, 17, e2024MS004232, https://doi.org/10.1029/2024MS004232, 2025.

https://doi.org/10.5194/egusphere-2025-6541
Preprint. Discussion started: 12 February 2026

779 Zhang, R., Xu, X., and Wang, Y.: Impacts of Subgrid Orographic Drag on the Summer
780 Monsoon Circulation and Precipitation in East Asia, Journal of Geophysical
781 Research: Atmospheres, 125, e2019JD032337,
782 https://doi.org/10.1029/2019JD032337, 2020.
783 Zhong, S., and Chen, Z.: Improved wind and precipitation forecasts over South China using
784 a modified orographic drag parameterization scheme, Journal of Meteorological
785 Research, 29, 132-143, https://doi.org/10.1007/s13351-014-4934-1, 2015.
786